Schweizerische Eidgenossenschaft
Confédération suisse
Confederazione Svizzera
Confederaziun svizra

Department of the Environment, Transport, Energy and Communication DETEC

Swiss Federal Office of Energy SFOE
Energy Research

Final report

Investigation of High Pressure Polymer Electrolyte Water Electrolysis

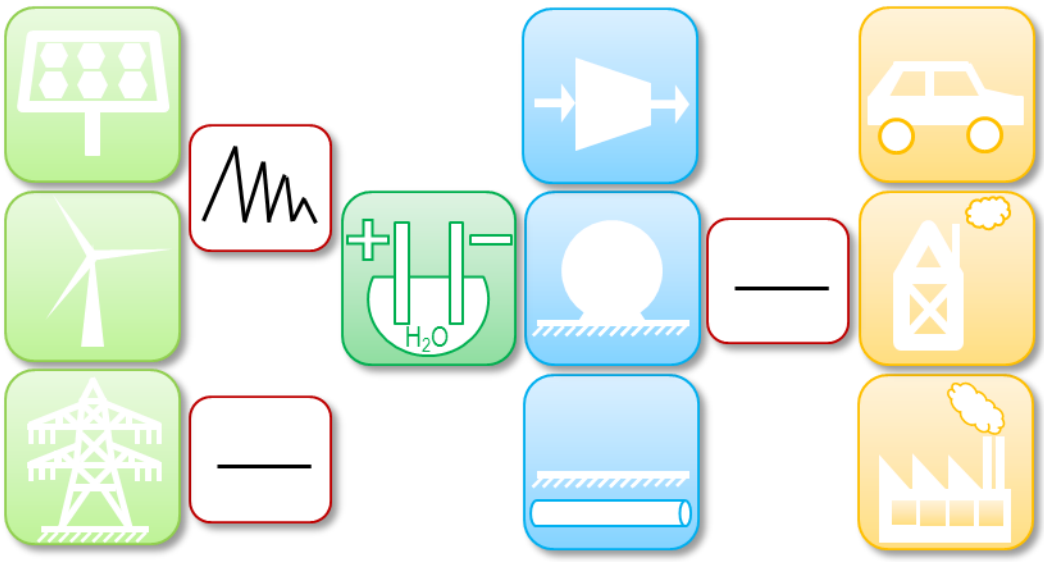

Date: 19. 12. 2016
Town: Villigen PSI

Publisher:
Swiss Federal Office of Energy SFOE
Hydrogen and Fuel Cells Research Programme
CH-3003 Bern
www.bfe.admin.ch

Co-financed by:
Belenos Clean Power Holding Ltd
Rue des Sors 3
CH-2074 Marin-Epagnier
http://www.belenoscleanpower.com

Agent:
Paul Scherrer Institut
5232 Villigen PSI
http://www.psi.ch/

Author:
Michel Suermann, Paul Scherrer Institut, michel.suermann@psi.ch
Felix Büchi, Paul Scherrer Institut, felix.buechi@psi.ch

SFOE head of domain: R. Schmitz, rolf.schmitz@bfe.admin.ch
SFOE programme manager: S. Oberholzer, stefan.oberholzer@bfe.admin.ch
SFOE contract number: SI/500904-01

Swiss Federal Office of Energy SFOE
Mühlestrasse 4, CH-3063 Ittigen; postal address: CH-3003 Bern
Phone +41 58 462 56 11 · Fax +41 58 463 25 00 · contact@bfe.admin.ch · www.bfe.admin.ch

Zusammenfassung

Zu Beginn wurde eine systematische Gefahren- und Betriebsfähigkeitsanalyse (HAZOP) durchgeführt, um die Risiken einer unter Druck (100 bar plus Sicherheitsfaktor von drei) betriebenen Polymerelektrolyt-Wasserelektrolyse (PEWE) abzuschätzen. Basierend auf der HAZOP wurden ein Teststand und eine Elektrolysezelle konstruiert und in Betrieb genommen. Mithilfe des Hochdruck-Testands konnten verschiedene Materialkombinationen elektrochemisch als Funktion der Temperatur (30 bis 70 °C), des Drucks (bis 100 bar) und der Stromdichte (bis zu 4 A/cm^2) untersucht werden. Hierfür wurden Strom-Spannungs Kennlinien und Hochfrequenzmessungen durchgeführt. Mithilfe eines Tafel-Modells wurde zwischen den drei Hauptüberspannungen (Kinetik, Ohm und Massentransport) unterschieden. Wie erwartet, nehmen alle drei Überspannungen mit der Stromdichte zu, wobei Massentransportverluste ab ca. 0.2 A/cm^2 auftreten. Bezüglich des Einflusses des Drucks, wird ein isothermisches Kompressionsverhalten, basierend auf der Thermondynamik, erwartet. Während dies für den Differenzdruck zutrifft, wird bei Gleichdruck ab einer relevanten Stromdichte von 1 A/cm^2 die Zellspannung zunehmend unabhängig vom Druck. Folglich müssen vorteilhafte Prozesse stattfinden. Diese konnten hauptsächlich einer verbesserten Kinetik zugeordnent werden. In Bezug auf die Kompressionsverluste wurden sowohl Verluste auf der Zellspannungsebene als auch Verluste durch den Gasdurchtritt durch die Membran betrachtet. Zwar sind die Verluste infolge des Gasdurchtritts für den Gleichdruckbetrieb nahezu doppelt so hoch im Vergleich zum Differenzdruckbetrieb, doch bewirken die vorteilhaften Prozesse letztendlich verringerte Kompressionsverluste über einen grossen Druckbereich, zumindest für höhere Stromdichten.

Summary

Initially, a systematical hazard and operability (HAZOP) study was performed to evaluate the risks for pressurized polymer electrolyte water electrolysis (PEWE) operation in the order of 100 bar with a safety factor of three. Based on the results of the HAZOP a test bench and an electrolysis cell were designed and commissioned. With the high pressure test bench, different material combinations were electrochemically investigated as a function of temperature (30 to 70 °C), pressure (up to 100 bar) and current density (up to 4 A/cm^2) by recording current-voltage characteristics and high frequency resistance (HFR) measurements. Furthermore a zero order model according to Tafel was applied to distinguish between the three main overpotentials: kinetic, ohmic and mass transport. As expected, all overpotentials increase with increasing current density, the mass transport overpotential occurs above around 0.2 A/cm^2. With respect to the pressure, isothermal compression behavior is expected from thermodynamics. While this holds true for differential pressure operation, for balanced pressure operation and at relevant current densities above around 1 A/cm^2 the cell voltage is increasingly independent of the balanced pressure. Consequently beneficial processes have to take place which could be mainly related with improved oxygen evolution kinetics. Concerning the compression losses, losses on the cell voltage level and losses due to gas crossover were considered. Even if the gas crossover losses are almost doubled for the balanced pressure compared to the differential pressure operation, it can be shown that balanced pressure operation ia energetically equal or even more beneficial for a wide pressure range, especially at higher current densities, due to the beneficial processes.

Contents

Project goals

The project aims to achieve a better understanding of the influence of pressure and dynamics on polymer electrolyte water electrolysis performance and efficiency. The influence of operating conditions such as current density, temperature and pressure are considered. Furthermore membrane and porous transport layer characteristics are studied with respect to the cell performance. Therefore, a test bench including an electrolysis cell have been engineered and put into operation. Last but not least the ideal way with respect to efficiency to compress hydrogen for obtaining hydrogen at pressure levels relevant for mobility applications is investigated.

The work is conducted in a PhD thesis which started on Jan 1st 2014.

Introduction and motivation

Polymer electrolyte water electrolysis (PEWE) is used to convert electrical excess energy into chemical energy by splitting water into hydrogen and oxygen to avoid curtailment (1). Depending on the application, the gases need to be compressed, e.g. for mobility up to 1000 bar. Conventionally, mechanical compression is used which causes significant (maintenance) costs. To reduce the compression and drying effort, commercial PEWE systems are operated in the order of 30 to 50 bar (2). Demonstrations for hydrogenpressure (differential), up to 700 bar (3, 4), or balanced pressure, up to 130 bar (5), have been demonstrated. However, also the electrochemical compression causes additional losses which can be related to an increased gas crossover (faradaic losses) and an increased cell voltage (thermodynamics). While the latter holds true for differential pressure operation and electrochemical hydrogen compressors (6), experimental data for balanced pressure operation show a different behavior where the cell voltage seems to be independent of the operating pressure, at least at relevant current densities. This unexpected behavior is investigated (7) and experiments designed and executed to gain fundamental knowledge about the influence of pressure with respect to all cell components and respective overpotentials. This understanding will enable the development of more efficient PEWE.

1 Experimental

The first work package deals with the challenges of a high pressure polymer electrolyte water electrolysis (PEWE) test bench. First the potential risks are discussed which were considered in a hazard and operability study (HAZOP). The outcome of the HAZOP is then the basis for the test bench design, which is discussed in the second part based on a piping and instrumentation diagram (PID). In the third and last part of this work package the design and working principle of the small scale electrolysis cell is described and special cell characteristics are highlighted.

1.1 Safety

At first a HAZOP was performed for PEWE operation in the order of 100 bar with a safety factor of three. Hazard sources like the pressure itself, possible combustible gas mixtures among others were considered. For instance, the lower explosion limit (LEL) of H_2 in O_2, which is at about 4 mol% at standard conditions and increases with pressure and slightly decreases with temperature (8), needs to be avoided. Based on the systematical HAZOP, a piping and instrumentation diagram (PID), a control software and work instructions were finalized.

1.2 Test bench environment

The PID of the electrolysis test bench is presented in Fig. 1. It can be devided into three main zones which are indicated by the labeling. The first one represents linking and auxiliary equipment, the second and third one are for the oxygen and hydrogen loops, respectively. Usually 6 mm (1 mm wall thickness) pipings from staineless stell (316L) is used.

Through the dosing pump (E-1.2, FLUSYS GmbH, DE), deionized water (<1 µS·cm^{-1}) is fed at the anode side. Subsequent the water is recirculated by a diaphragm pump (E-2.1, LEWA GmbH, DE) with a defined water flow up to 120 mL/min. Contrary, at the cathode natural convection takes place.

To minimize the influence of the corrosive behavior of the deionized water, an in-house designed ion exchanger is implemented in the anode loop (E-2.4) using a mixed ion resin bed (LEWATIT® MonoPlus S 108 H and MP 62, Chemia Brugg, CH).

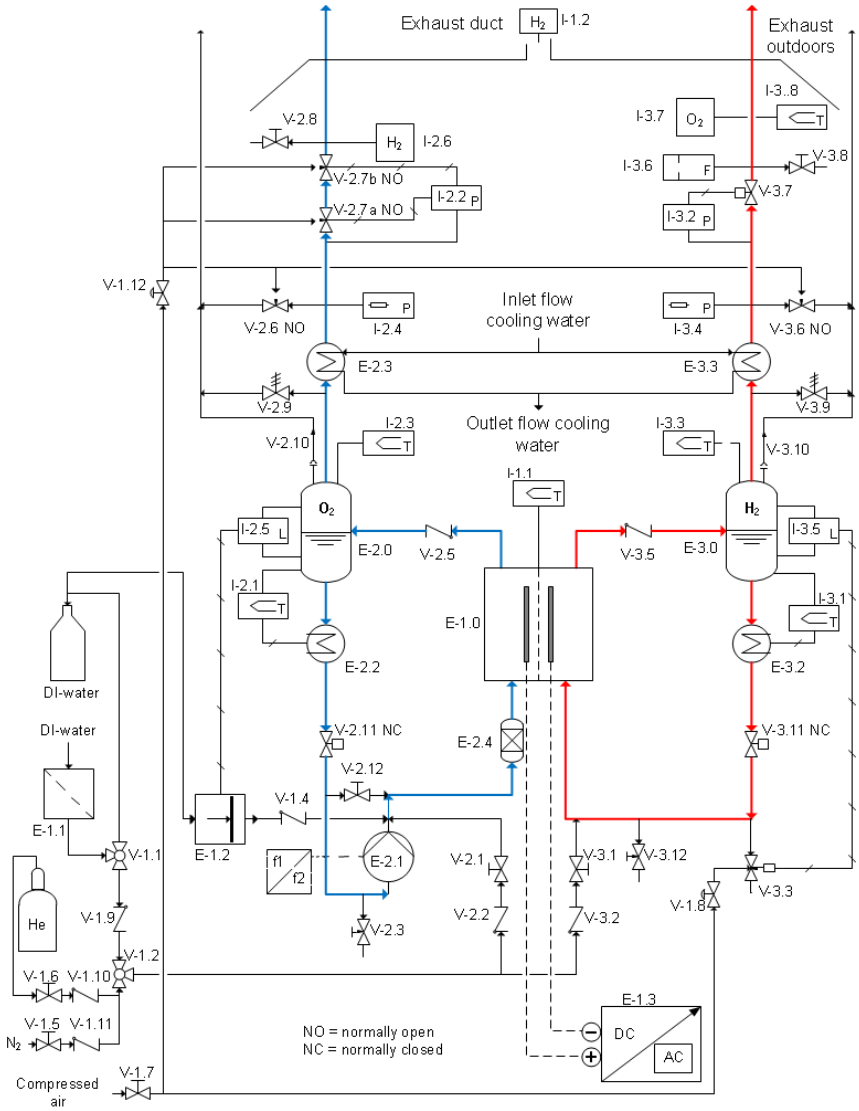

Figure 1: PID of the 100 bar water electrolysis test bench. Labeled as follows: valves (V), instruments (I) and equipment (E) as well as 1.x for linking and auxiliary components, 2.x for the oxygen path and 3.x for the hydrogen path.

After splitting the water in the electrolyzer cell (E-1.0), the gases are separated from the excess water (anode) and from the electro-osmotic drag water (cathode) in gas/liquid separators (E-2.0/3.0, SITEC-Sieber Engineering AG, CH). To control the water level inside the separators, impedance sensors (I-2.5/3.5, Aquasant Messtechnik AG, CH) are used. While the anodic level sensor feedback is used for the inlet pump (E-1.2), the cathodic equivalent is used for the outlet valve (V-3.3).

Figure 2: Image of the test bench.

Regarding the pressure, both operation modes (balanced and differential) are possible by using separate pressure controls (I-2.2/3.2, V-2.7/3.7, Bronkhorst, CH). Pressure pulses in the order of 1% of the operating pressure, caused by the recirculating pump, had to be managed. To resolve pressure stability problems an in-house pressure control system with two pneumatic valves (SITEC-Sieber Engineering, CH) working with alternating openings was installed.

Furthermore several sensors and valves are implemented to conform to the HAZOP. Therefore hydrogen is measured in the oxygen outlet (I-2.6, BlueSens gas sensor, DE) and oxygen in the hydrogen outlet (I-3.7, GHM Messtechnik, DE). In case of an undesired incident with respect to pressure, redundant analog pressure sensors (I-2.4/3.4, Brooks Instrument, US), explosion disks (V-2.10/3.10), overpressure valves (V-2.9/3.9) and pneumatic normally open security valves (V-2.6/3.6, all SITEC-Sieber Engineering, CH) are installed. A picture of the test bench is shown in Fig. 2.

1.3 Electrolysis cell

The PEWE single cell (E-1.0) was designed in-house with support of a specialized company (SITEC-Sieber Engineering, CH) for solving gasket issues. It is based on a small scale concept with an active area of 4 cm^2 to reduce any gradients along the flow field channels. Thus later no effects in flow directions have to be condisered for the electrochemical characterization.

As shown in Fig. 3, a catalyst coated membrane (CCM, Nafion 117CS or Nafion 212, E400, from Greenerity®, DE) is embedded between two porous titanium sintered powder materials (SIKA T series, GKN Sinter Metals Filters, DE) which are used as the porous transport layers (PTLs). The choice of material is limited due to high electrochemical potential, at least for the anode (9). Next to the PTLs straight channel type flow-fields, housed in a distributer plates are placed. In this work flow fields with 5 straight parallel channels (1 mm height, 2 mm width) and 2 mm ribs were used.

While the compression of the flat gasket area between the endplates and distributor plates (see Fig. 3) as well as between the distributer plates and the CCM is induced by the outer screws, the compression of the active area is applied by a set of springs inside the cathode side. Thus a homogeneous and a defined contact pressure is possible (here 2.5 MPa is used).

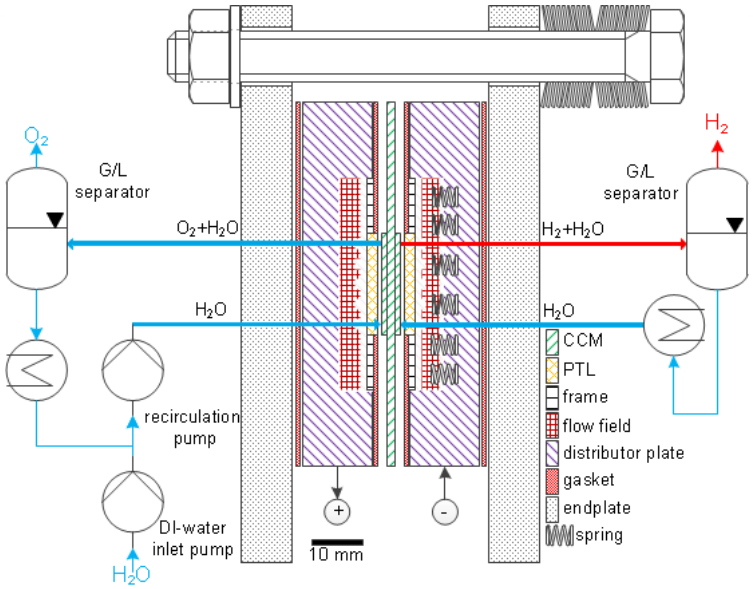

Figure 3: Schematic drawing of the high pressure polymer electrolyte single electrolyzer cell.

The flow fields, distributor and end plates are made from stainless steel (1.4571), the springs from spring steel and protected by a galvanic coating (10 µm gold on a nickel undercoating, Silbag, CH) to avoid corrosion and to ensure sufficient electrical contact.

For temperature control of the cell, heat exchangers (E-2.2/3.2) are implemented and the cell temperature is measured by a thermocouple (I-1.1) inside a drill hole in the distributor plate close to the active area.

2 Theory and overpotential analysis

In this chapter the applied electrochemical overpotential analysis based on a zero order model according to Tafel is described. The section is an excerpt from the first published paper of this work (10) and reprinted with permission from Elsevier.

The voltage of the electrolysis cell *E* can be considered as the sum of the thermodynamic cell voltage $E^0(p,T)$ and the three main overpotentials:

$$E = E^0(p,T) + \eta_{iR} + \eta_{kin} + \eta_{mtx} \tag{1}$$

where η_{iR} denotes the ohmic, η_{kin} the kinetic and η_{mtx} the mass transport overpotential, respectively. In eq. (1) the thermodynamic cell voltage $E^0(p,T)$ is calculated from the Nernst equation:

$$E^0(p,T) = E^0(T) + \frac{R \cdot T}{2 \cdot F} \ln\left(\frac{a(H_2) \cdot \sqrt{a(O_2)}}{a(H_2O)} \right) \tag{2}$$

with *a* the activity of the species and $E^0(T)$ the temperature dependent equilibrium potential (11).

Since the solubility of hydrogen and oxygen in water is linear up to 100 bar, ideal gas behavior for both H_2 and O_2 can be assumed, because at thermodynamic equilibrium conditions only the dissolved gas in the water is in contact with the electrodes (12). Consequently, the activity can be expressed by the partial pressure. The activity of water is assumed as unity.

The ohmic overpotential η_{iR} is obtained from the HFR measurement and represents the sum of the ionic and electronic ohmic losses. By subtracting the ohmic overpotential from the cell voltage, the iR-free cell voltage is obtained. The iR-free cell voltage shows a Tafel behavior at low current densities i.e. a linear semi-logarithmic behaviour is observed. To the linear regions, the Tafel line can be fitted as described by eq. (3):

$$\eta_{kin} = b \cdot \log\left(\frac{j}{j_0}\right) \tag{3}$$

where the kinetic overpotential η_{kin} is equal to the difference between the Tafel line and the thermodynamic cell voltage according to eq. (2), b is the Tafel slope, equal to $2.3 \cdot R \cdot T/(\alpha \cdot F)$, and α is the transfer coefficient, a constant related to the mechanism of the electrochemical reaction including the number of transferred electrons and j_0 is the apparent exchange current density.

Consequently the mass transport overpotential η_{mtx} is defined as the difference between the iR-free cell voltage and the Tafel line. A detailed description can be found in (10).

3 Influence of the membrane and porous transport layer

The work package 3 discusses the influence of different materials with respect to the cell performance. In the first section the influence of the membrane thickness is shown. In the second and main section the influence of the porous transport layer (PTL) is discussed. Here only commercial products were investigated by using current voltage characteristics (i/E-curves) from 1 to 4000 mA/cm^2 and high frequency resistance (HFR) measurements, recorded at 25 kHz. The different overpotentials were distinguished according to the overpotential analysis described in chapter 2.

3.1 Membrane

For the same type of membrane, reducing its thickness reduces the ionic ohmic overpotential and increases the gas crossover. Thus, depending on the application, a compromise between those opposing trends has to be found. In Fig. 4 the i/E-curves for a relatively thick membrane (Nafion 117, ≈200 µm) and a relatively thin membrane (Nafion 212, ≈60 µm) are compared.

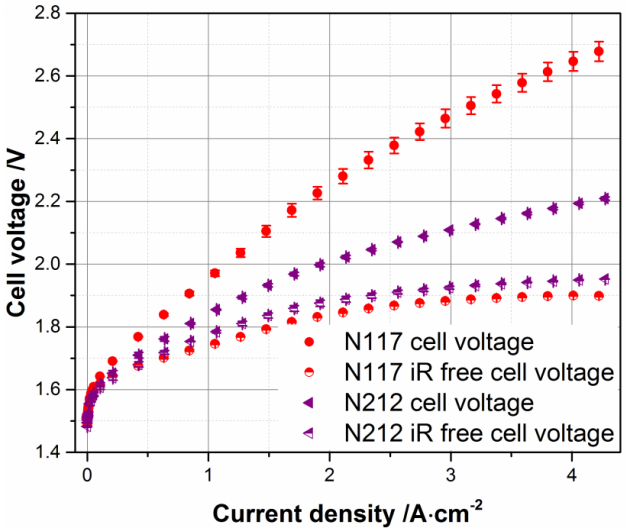

Figure 4. (IR-free) cell voltage for Nafion 117/212 at 50 °C and 10 bar balanced gas pressure. Figure is taken from publication (10) with permission from Elsevier.

3.2 Porous transport layer

In this section three different porous transport layers (PTLs) made of sintered titanium powder and two different thicknesses are characterized in cell experiments. Below in chapter 4 the so far best performing material is investigated in detail with respect different operating parameters.

By comparing three different PTLs at 50 °C and 10 bar balanced pressure a significant difference only in the mass transport overpotential was observed as shown in Fig. 5. It can be seen that T10 is clearly better performing (lower overpotetials) as compared to T5 and especially to T20. For instance at 1 A/cm^2, the mass transport overpotentials for T5, T10 and T20 (all 1 mm thickness) are 60, 35 and 80 mV, respectively. Increasing the thickness of T10 from 1 to 2 mm increases the transport losses by roughly 50%.

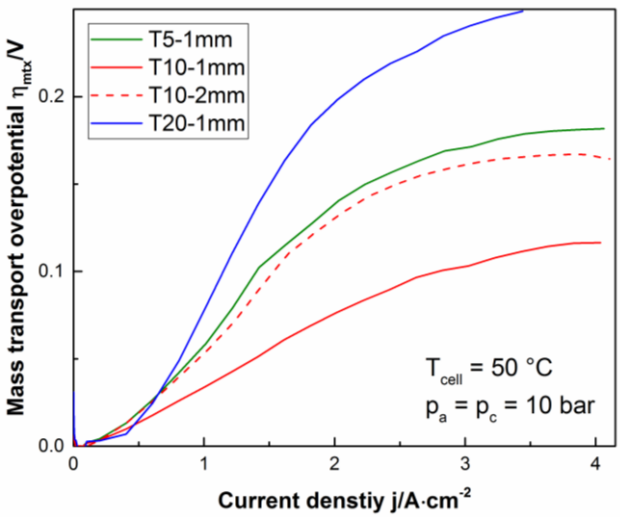

Figure 5. Mass transport overpotentials for T5, T10 (1 and 2 mm thickness) and T20 at 50 °C and 10 bar balanced pressure.

4 Overpotentials as a function of current density, temperature and pressure

In this chapter the influence of the current density, temperature and pressure on the electrolysis performance is investigated. The presented results are presented in one sub-section each for theohmic, mass transport and kinetic overpotentials. This chapter section is an excerpt from the first paper published in this project (10) and reprinted with permission from Elsevier.

4.1 Ohmic overpotential

The ohmic losses mainly consist of the proton transport resistance in the membrane and the influence the membrane thickness towards the performance was already shown in Fig. 4. Regarding the pressure, little to no influence was observed with respect to the ohmic overpotential, indicated by the HFR measurements, as shown in Fig. 6a. Contrary the cell temperature and the waste heat production due to the overpotentials significantly influence the HFR and thus the performance of the electrolyzer. For a more detailed analysis please read our published work (10).

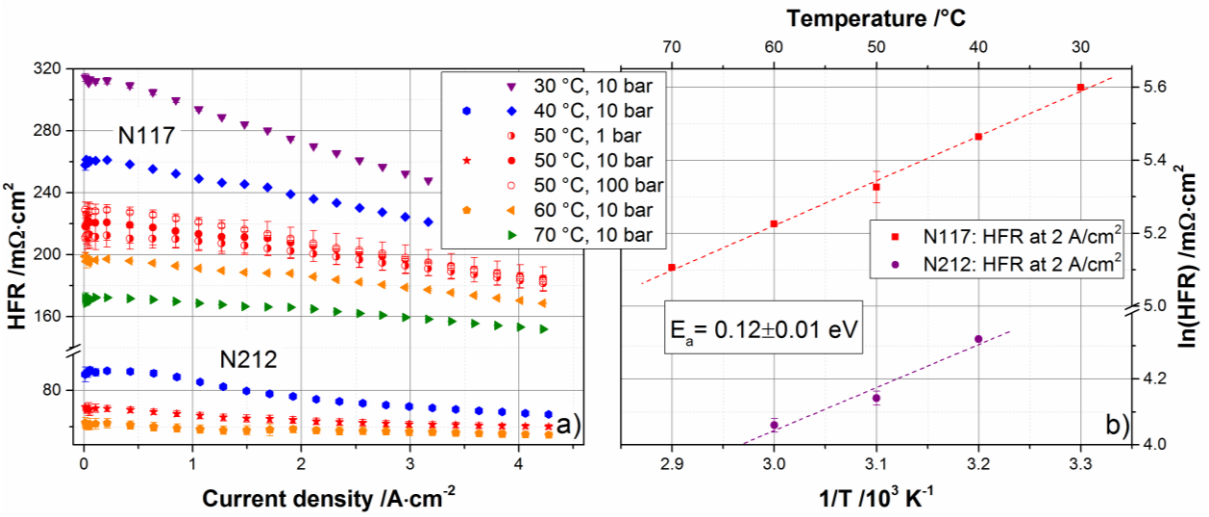

Figure 6. a) HFR measurements of Nafion 117 and Nafion 212 for different cell temperatures and operating pressures as a function of current density; b) Arrhenius plot of the HFR data at 2 A/cm^2 and 10 bar, for the data in sub-plot a). Figure is taken from (10) with permission from Elsevier.

4.2 Mass transport overpotential

The iR-free cell voltage for 1, 10 and 100 bar at 50 °C is plotted semi-logarithmically vs. the current density in Fig. 7a. At current densities up to about 200 mA/cm^2, the expected, linear voltage behavior is observed indicating that no mass transport losses occur. Furthermore, at low current densities the cell voltage increases with increasing pressure as expected from thermodynamics, with increasing current however, the cell voltages coincide at around 1 A/cm^2.

At higher current densities, cell voltages are practically independent of pressure, but clearly an offset of the iR-free cell voltage from the extrapolated Tafel line is seen. This difference increases with current density to about 150 mV up to 4 A/cm^2. This loss is considered the mass transport overpotential. It increases monotonically with current, but flattens out at current densities above 2 A/cm^2.

The effect of pressure on the mass transport loss is summarized in Fig. 8a. Above 3 A/cm^2, the mass transport overpotential decreases slightly from around 170 to 140 mV for the pressure increase from 1 to 100 bar.

The influence of temperature on the mass transport losses (Fig. 7b) is analyzed in Fig. 8b. A temperature increase from 30 to 70 °C results in a decrease in transport overpotential from 200 to 100 mV above 2 A/cm^2.

When water transport in the gas phase contributes to the mass transport overpotential, the temperature effect may be due to the changing water partial pressure. In case liquid transport is critical and limiting, the decreasing viscosity and/or surface tension of liquid water may play a role. Furthermore the change of wettability of the hydrophilic pores of the PTL and/or CL (13) can have an influence. However, the effects of these potential causes cannot be separated with the present data and needf further investigation.

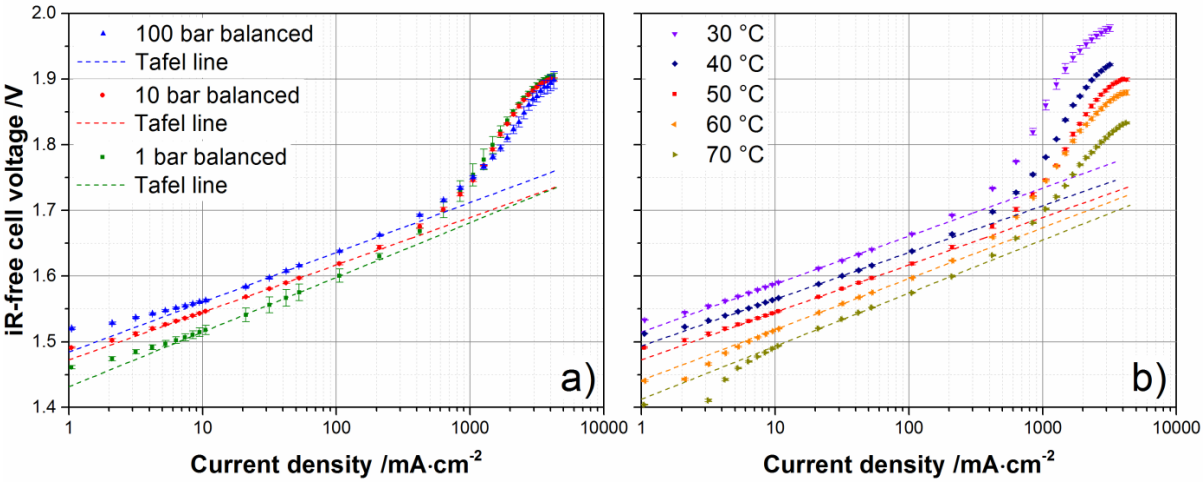

Figure 7. Tafel plots of Nafion 117 for different temperatures and pressures; a) for 1, 10 and 100 bar at 50 °C and b) for 30 to 70 °C at 10 bar. Figure is taken from own published work (10) with permission from Elsevier.

Summarizing, it can be stated that mass transport contributes to the cell voltage starting at current densities above 200 mA/cm^2, reaching 100 to 200 mV at 2 A/cm^2. Reasons of the mass transport losses are not clear, but it seems obvious that the two phase flow at the anode plays a decisive role.

4.3 Kinetic overpotential

The kinetic overpotential is calculated from the difference between the fitted Tafel lines (as in Fig. 7) and the thermodynamic cell voltage calculated according to eq. (2). Typically, the anodic kinetic overpotential is significantly higher than the cathodic due to the sluggish oxygen evolution reaction (14). The value of the thermodynamic cell voltage is influenced by the activities of gases and water in equation (2). Assuming ideal gas behavior and an activity of unity for the liquid water, at 50 °C, an increase of the thermodynamic voltage of 48 mV/dec of pressure is expected.

However the measured iR-free cell voltage difference between 1 and 100 bar at 10 mA/cm^2 is only 23 mV/dec (see Fig. 7a), which indicates that either the assumptions for the activities are not correct or even at small current densities processes, not described by thermodynamics, take place.

The different overpotentials are summarized in Fig. 8a as function of pressure at 50 °C and in Fig. 8b as function of temperature at 10 bar. Increasing the pressure decreases the kinetic and transport overpotentials, while increasing cell temperature reduces all three loss mechanisms.

In Fig. 8 it can be seen that for cells with Nafion 117 membranes, the kinetic overpotential is the dominant loss up to a current density of about 2 A/cm^2. With thinner membranes this range is shifted to higher current densities. The mass transport overpotential plays a minor role at low current densities. However in the commonly used operation range of 1 to 3 A/cm^2 it contributes 10 to 15% of the overall overpotential. For thinner membranes it will contribute a higher fraction in the same current density range.

Table 1. Summary of the contributions of the kinetic and mass transport overpotentials at 100 bar (as compared to 1 bar operation) to the difference in the cell voltage for selected current densities. Table is taken from (10) with permission from Elsevier

j	**A/cm^2**	**0.001**	**0.01**	**0.1**	**0.4**	**1**	**4**
$\Delta E^0(p,T)$	mV	96	96	96	96	96	96
$\Delta\eta_{kinetic}$	mV	-43	-51	-58	-63	-66	-70
$\Delta\eta_{mass\ transport}$	mV	6	-1	0	-9	-34	-36
ΔE_{cell}	mV	59	44	38	24	-4	-10

The fact that the kinetic and transport overpotentials drop with pressure is further illustrated by the values given in Table 1. Negative values indicate a reduction of the overpotentials with increase of the gas pressure from 1 to 100 bar.

The data in Table 1 show that only at low current densities a higher cell voltage is observed with the pressure increase over two decades. However, the raise in cell voltage is less than predicted by theory for an activity of liquid water equal to one. With increasing current densities the beneficial influences of mass transport and kinetics are more and more compensating the higher thermodynamic cell voltage. Finally at the highest current densities the cell voltage even slightly drops with increasing pressure. At low current densities the kinetics contribute most to cell voltage reduction. At current densities of 1 A/cm^2 and larger the transport contributes about one third to the overall beneficial effects.

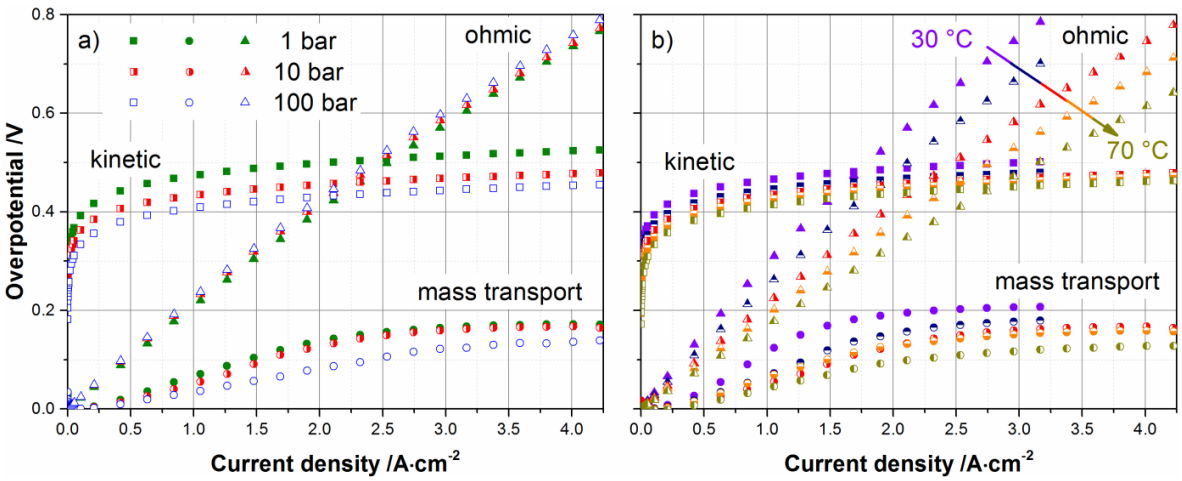

Figure 8. Contributions of kinetic, ohmic and mass transport overpotentials for Nafion 117 as a function of current density; a) at 50 °C for 1,10 and 100 bar and b) at 10 bar for 30, 40, 50, 60 and 70 °C. Figure is taken from own published work (10) with permission from Elsevier.

5 Compression loss and compression strategy

This chapter focusses on the energetic hydrogen compression loss for pressurized electrolysis as a function of current density and pressure operation, i.e. balanced or differential pressure. For a wider context, the results are compared to modern mechanical hydrogen compressors.

Since the ohmic overpotential is independent of the pressure (see Fig. 8a), only the iR-free cell voltage is further processed. Thus in Fig. 9 the iR-free cell voltage at 50 °C for ambient pressure, 30 bar differential and balanced pressure are compared. According to eq. 2, by increasing the oxygen and/or hydrogen pressure, also an increase in the cell voltage is expected due to the increasing thermodynamic cell voltage. This holds largely true for the *differential* pressure operation (compression of hydrogen only), i.e. isothermal compression behavior is confirmed. Contrary, as the current density increases, the iR-free cell voltage for 30 bar *balanced* pressure converges to the ambient pressure curve.

For an overall analysis, besides the performance related compression losses, additional losses due to gas crossover have to be considered. For the *differential* pressure operation only the hydrogen gas crossover has to be taken into account. Contrary, for the *balanced* pressure operation also the oxygen gas crossover which is about half of that of hydrogen has to be considered (15). When assuming that all oxygen diffused to the cathode, recombines (Pt-based catalyst) with hydrogen back to water, the total loss due to gas crossover is about doubled (as compared to differential operation).

For Nafion 117 the loss due to hydrogen gas crossover can be expressed as an equivalent current density, normalized to the partial pressure, which is about 0.3 $mA \cdot cm^{-2} \cdot bar^{-1}$ at 55 °C (15). For extrapolation towards higher pressures, a gas crossover behaviour according to Fick's law of diffusion is assumed.

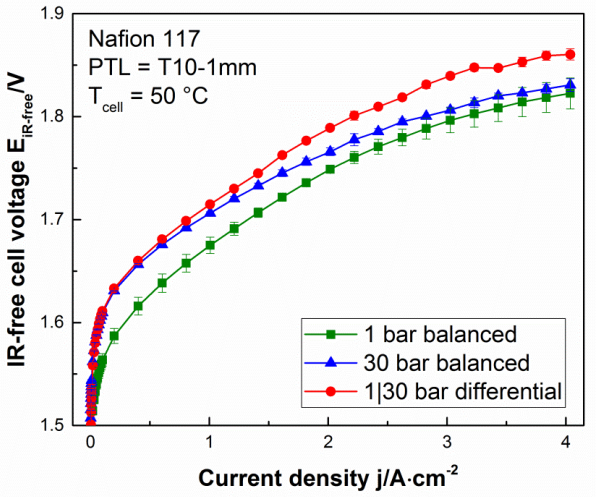

Figure 9. IR-free cell voltage at 50 °C for ambient, 30 bar differential and balanced pressure.

When the cell voltage loss is merged together with the gas crossover losses, a compression loss, normalized to the lower heating value (LHV) of hydrogen (240 kJ/mol) can be calculated. Assuming that the experimental findings from Fig. 9 can be extrapolated towards lower and higher pressures (e.g. Fig. 7), the compression losses for *differential* and *balanced* pressure opeartion can be calculated as a function of the current density (1 and 2 A/cm^2) up to 1000 bar hydrogen pressure. Results are shown in Fig. 10. Here only the produced hydrogen is of interest, but still the loss due to oxygen gas crossover is considered for the balanced pressure operation. Furthermore the actual difference in the iR-free cell voltage between the pressurized and the ambient pressure operation

(data from Fig. 9) and their ratio with respect to the theoretical thermodynamic cell voltage increase of (ΔE^0(p,T) = 47 mV) are summarized in Table 2.

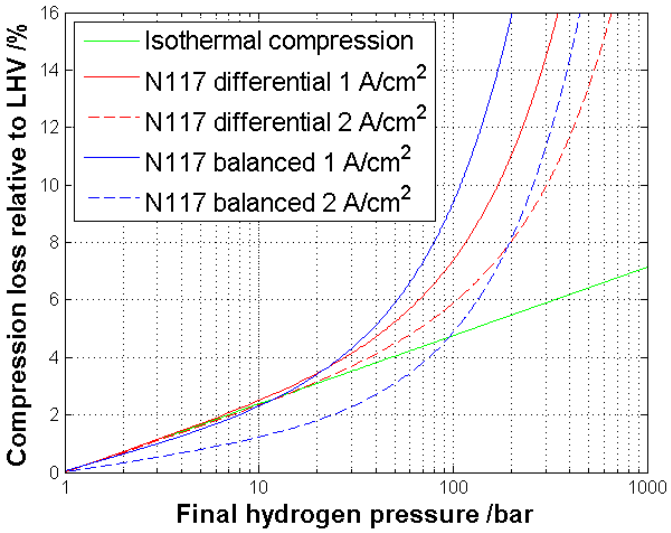

Figure 10. Compression loss relative to the LHV of hydrogen for isothermal compression (25 °C), differential and balanced pressure PEWE operation at 50 °C using Nafion 117. The solid and dashed lines correspond to an applied current density of 1 and 2 A/cm^2, respectively.

Based on the data presented in Fig. 10 several observations can be formulated:

- At low compression factors below about 10, losses according to the isothermal compression are dominant.
- Above around 10 bar, losses due to the gas crossover become more and more important. Thus the shape of the curves changes from linear to exponential (in the semi-logarithmic plot).
- Because the differential pressure mostly follows isothermal compression behaviour, the difference in the compression loss between 1 and 2 A/cm^2 is rather small compared to balanced pressure.
- Regarding relatively small current densities (here 1 A/cm^2), the total compression loss is less for differential pressure operation.
- Contrary for higher current densities (here 2 A/cm^2), it seems preferable to use balanced pressure operation, even up to a relatively high pressure of about 150 bar, because the pressure induced beneficial processes on the cell voltage level compensate for the doubled loss due to gas crossover. However, for higher hydrogen pressures differential pressure operations become more and more advantageous.

Table 2. Difference in the iR-free cell voltage between pressurized and ambient pressure operation and their ratio towards the theoretical thermodynamic voltage increase (ΔE^0(p,T)=47 mV).

	$\Delta E_{iR\text{-}free}$ towards ambient at 1 A/cm^2	Ratio of $\Delta E^0(p,T)$	$\Delta E_{iR\text{-}free}$ towards ambient at 2 A/cm^2	Ratio of $\Delta E^0(p,T)$
30 bar differential	40 mV	85%	40 mV	85%
30 bar balanced	31 mV	66%	17 mV	36%

Furthermore the energetic compression loss of the above discussed differential and balanced pressure PEWE can be compared with mechanic hydrogen compressors which are ideally following an isothermal compression behavior too. New 5-stage ionic compressors of Linde (16) are claimed to consume 2.7 kWh/kg of hydrogen for a compression ratio of 180. At standard conditions this energy consumption corresponds to a compression loss of about 8.1% compared to a theoretical isothermal compression loss of 5.3%. Thus it is preferable to use electrochemical compression (balanced or differential pressure) PEWE up to around 50 bar (at 1 A/cm^2) or up to around 150 bar (at 2 A/cm^2). For higher hydrogen pressure levels, from an energetic point of view (with the Nafion membrane materials), a subsequent mechanical compression is more efficient.

However, so far the both pressure concepts were just discussed from an energetic point of view regarding the compression loss due to the electrochemical performance and due to the gas crossover for a specific material and operating parameter choice. For commercial PEWE systems even more parameters have to be considered, e.g. the purity of the gases, dew-point of the gases, capex vs. opex, asf. This would be a study on its own.

Outlook

Especially the origin of the transport losses and the influence of the porous transport and the catalyst layers as well as their interface are still not well understood. Here additional measurement techniques, e.g. based on imaging, might be helpful to better understand the effects and design more efficient electrolyzers.

Another open question refers towards the pressure induced improved kinetics. So far it can be related to the apparent exchange current density, but if it is the specific exchange current density and/or roughness factor which changes with pressure is not clear. Furthermore if the beneficial process(es) of the balanced pressure operation are a function of the catalyst material and morphology is unclear.

Nevertheless, the total (compression) loss from the production to the application of hydrogen is of interest in the end of the day. Here studies based on commercially relevant systems considering the production, compression, drying, purification, transport, storing, etc. are needed.

National cooperation

There has been close knowledge exchange with Belenos Clean Power in regular meetings. Especially the exchange of fundamental results on the lab scale compared with experiences in commercial applications on the system scale was beneficial for the project.

Publications and talks

The project has resulted in the following papers and conference presentations:

Peer-reviewed papers

2016 M. Suermann, T.J. Schmidt and F.N. Büchi, *Cell Performance Determining Parameters in High Pressure Water Electrolysis*, EACTA (doi: 10.1016/j.electacta.2016.06.120)

2016 U. Babic, M. Suermann, F.N. Büchi, L. Gubler and T.J. Schmidt, *Identifying Critical Gaps for Polymer Electrolyte Water Electrolysis Development*, JES (submitted)

2016 M. Suermann, A. Patru, T.J. Schmidt, F.N. Büchi, *High Pressure Polymer Electrolyte Water Electrolysis: Test Bench Development and Electrochemical Analysis*, IJHE (submitted)

Planned peer-reviewed papers until finalization of the thesis in June 2017:

i) "mass transport losses vs. PTL" → mainly results from chapter 3

ii) "hydrogen compression loss" → mainly results from chapter 5

Conference paper

2015 M. Suermann, T.J. Schmidt and F.N. Büchi, *Investigation of Mass Transport Losses in Polymer Electrolyte Electrolysis Cells*, ECS Trans. (doi: 10.1149/06917.1141ecst)

Conference posters (underlined name represents the presenter)

2014 Michel Suermann, Thomas J. Schmidt, Felix N. Büchi, Electrochemistry, Mainz, *Experimental Investigation of Mass Transport Losses in Polymer Electrolyte Electrolysis Cells*

Talks (underlined name represents the speaker)

2015 Michel Suermann, Thomas J. Schmidt, Felix N. Büchi, ECS, Glasgow, *Experimental Investigation of the Influence of Pressure on the Performance of Polymer Electrolyte Water Electrolysis Cells*

2015 Michel Suermann, Thomas J. Schmidt, Felix N. Büchi, ECS, Phoenix, *Investigation of Mass Transport Losses in Polymer Electrolyte Electrolysis Cells*

2016 Michel Suermann, Thomas J. Schmidt, Felix N. Büchi, 2nd Degradation workshop, Freiburg, *Analysis of Voltage Losses in Polymer Electrolyte Electrolysis Cells* (invited talk)

2016 Michel Suermann, Thomas J. Schmidt, Felix N. Büchi, ECS, Honolulu, *Overpotential Analysis in High Pressure Water Electrolysis*

References

1. C. J. Barnhart, M. Dale, A. R. Brandt and S. M. Benson, *Energy & Environmental Science*, **6**, 2804 (2013).
2. M. Felgenhauer and T. Hamacher, *International Journal of Hydrogen Energy*, **40**, 2084 (2015).
3. K. E. Ayers, E. B. Anderson, C. B. Capuano, B. D. Carter, L. T. Dalton, G. Hanlon, J. Manco and M. Niedzwiecki, *ECS Transactions*, **33**, 3 (2010).
4. H. Ishikawa, E. Haryu, N. Kawasaki and H. Daimon, *Honda R&D Technical Review*, **28** (2016).
5. S. A. Grigoriev, V. I. Porembskiy, S. V. Korobtsev, V. N. Fateev, F. Auprêtre and P. Millet, *International Journal of Hydrogen Energy*, **36**, 2721 (2011).
6. P. J. Bouwman, J. Konink, D. Semerel, L. Raymakers, M. Koeman, W. Dalhuijsen, E. Milacic and M. Mulder, *ECS Transactions*, **64**, 1009 (2014).
7. S. A. Grigoriev, M. M. Khaliullin, N. V. Kuleshov and V. N. Fateev, *Russian Journal of Electrochemistry*, **37**, 819 (2001).
8. V. Schröder, B. Emonts, H. Janssen and H.-P. Schulze, *Chemie Ingenieur Technik*, **75**, 914 (2003).
9. H. Ito, T. Maeda, A. Nakano, A. Kato and T. Yoshida, *Electrochimica Acta*, **100**, 242 (2013).
10. M. Suermann, T. J. Schmidt and F. N. Büchi, *Electrochimica Acta*, **211**, 989 (2016).
11. I. Barin and G. Platzki, Thermochemical Data of Pure Substances, in, p. 795, VCH Verlagsgesellschaft mbH, Weinheim (1995).
12. H. Ito, T. Maeda, A. Nakano and H. Takenaka, *International Journal of Hydrogen Energy*, **36**, 10527 (2011).
13. N. Pérez-Hernández, T. Q. Luong, M. Febles, C. Marco, H.-H. Limbach, M. Havenith, C. Pérez, M. V. Roux, R. Pérez and J. D. Martín, *The Journal of Physical Chemistry C*, **116**, 9616 (2012).
14. E. Brightman, J. Dodwell, N. van Dijk and G. Hinds, *Electrochemistry Communications*, **52**, 1 (2015).
15. M. Schalenbach, T. Hoefner, P. Paciok, M. Carmo, W. Lueke and D. Stolten, *The Journal of Physical Chemistry C*, **119**, 25145 (2015).
16. M. Stefan, in *20th World Hydrogen Energy Conference, WHEC 2014*, KDJ Convention Center Gwangju, South Korea (2014).